

Depletion of stromal cells expressing fibroblast activation protein- α from skeletal muscle and bone marrow results in cachexia and anemia

Edward W. Roberts,^{1,4} Andrew Deonarine,⁵ James O. Jones,^{1,4} Alice E. Denton,^{1,4} Christine Feig,⁴ Scott K. Lyons,⁴ Marion Espeli,² Matthew Kraman,^{1,4} Brendan McKenna,¹ Richard J.B. Wells,^{1,4} Qi Zhao,⁶ Otavia L. Caballero,⁶ Rachel Larder,³ Anthony P. Coll,³ Stephen O'Rahilly,³ Kevin M. Brindle,⁴ Sarah A. Teichmann,⁵ David A. Tuveson,^{4,7} and Douglas T. Fearon^{1,4}

¹Department of Medicine; ²Cambridge Institute for Medical Research, Wellcome Trust/Medical Research Council (MRC) Building; and ³Institute of Metabolic Sciences; Addenbrooke's Hospital; ⁴Cancer Research UK Cambridge Institute, Li Ka Shing Centre; and ⁵MRC Laboratory of Molecular Biology; University of Cambridge, Cambridge CB2 2QH, England, UK
⁶Ludwig Collaborative Laboratory, Johns Hopkins University School of Medicine, Baltimore, MD 21231
⁷Cold Spring Harbor Laboratory, Cold Spring Harbor, NY 11724

Fibroblast activation protein- α (FAP) identifies stromal cells of mesenchymal origin in human cancers and chronic inflammatory lesions. In mouse models of cancer, they have been shown to be immune suppressive, but studies of their occurrence and function in normal tissues have been limited. With a transgenic mouse line permitting the bioluminescent imaging of FAP⁺ cells, we find that they reside in most tissues of the adult mouse. FAP⁺ cells from three sites, skeletal muscle, adipose tissue, and pancreas, have highly similar transcriptomes, suggesting a shared lineage. FAP⁺ cells of skeletal muscle are the major local source of follistatin, and in bone marrow they express Cxcl12 and KitL. Experimental ablation of these cells causes loss of muscle mass and a reduction of B-lymphopoiesis and erythropoiesis, revealing their essential functions in maintaining normal muscle mass and hematopoiesis, respectively. Remarkably, these cells are altered at these sites in transplantable and spontaneous mouse models of cancer-induced cachexia and anemia. Thus, the FAP⁺ stromal cell may have roles in two adverse consequences of cancer: their acquisition by tumors may cause failure of immunosurveillance, and their alteration in normal tissues contributes to the paraneoplastic syndromes of cachexia and anemia.

CORRESPONDENCE
Douglas T. Fearon:
dtf1000@cam.ac.uk

Abbreviations used: BAC, bacterial artificial chromosome; CLP, common lymphoid progenitor; DTR, DTX receptor; DTX, diphtheria toxin; FAP, fibroblast activation protein- α ; FPKM, fragments per kilobase million; Fst, follistatin; HSC, hematopoietic stem cell; Lepr, leptin receptor; MEP, megakaryocyte-erythroid progenitor; Mstn, myostatin; PCA, principal component analysis; PDA, pancreatic ductal adenocarcinoma; pro-B, pro-B cell; pro-E, pro-erythroblast; qRT-PCR, quantitative RT-PCR; RPKM, reads per kilobase million; VST, variance-stabilized transform.

The membrane dipeptidyl peptidase fibroblast activation protein- α (FAP) was originally identified by the F19 monoclonal antibody derived from a mouse immunized with human lung fibroblasts. Using this antibody, it was originally reported that FAP was expressed by human astrocytomas (Rettig et al., 1986), but a second study refined this analysis and showed expression to be mainly by reactive fibroblasts in the tumor stroma of human adenocarcinomas and in healing dermal scars (Garin-Chesa et al., 1990). Since then, FAP⁺ stromal cells have been found also in chronic inflammatory lesions, such as primary biliary cirrhosis (Levy et al., 1999), atherosclerosis (Brokopp et al., 2011), and rheumatoid

arthritis (Bauer et al., 2006). These observations suggest that the inflammatory, wound-healing aspect of the tumor microenvironment (Dvorak, 1986) may account for the occurrence of FAP⁺ cells in the tumor stroma.

The presence of FAP⁺ stromal cells in tumors has stimulated three general lines of research related to tumor therapy. The first focuses on the enzymatic role of FAP itself rather than on the cell that expresses it. The evolutionary conservation

© 2013 Roberts et al. This article is distributed under the terms of an Attribution-Noncommercial-Share Alike-No Mirror Sites license for the first six months after the publication date (see <http://www.rupress.org/terms>). After six months it is available under a Creative Commons License (Attribution-Noncommercial-Share Alike 3.0 Unported license, as described at <http://creativecommons.org/licenses/by-nc-sa/3.0/>).

of FAP has led to a suggestion that it may have important functions (Park et al., 1999). FAP^{-/-} mice, however, have no striking phenotypes (Niedermeyer et al., 2000), inhibiting the dipeptidyl peptidase activity of FAP has only a modest effect on tumor growth in the mouse (Santos et al., 2009), and FAP inhibitors have not demonstrated clinical efficacy in humans (Eager et al., 2009a,b). The second line of research concerns the finding of selective uptake of an ¹³¹I-labeled, humanized form of the F19 antibody (sibrotuzumab) by tumors and not by normal tissues in patients with colorectal carcinoma or non-small cell lung cancer (Scott et al., 2003). This apparently restricted distribution of FAP⁺ cells suggested that cancer therapeutics can be localized to the tumor site by the use of either anti-FAP antibody conjugates (Hofheinz et al., 2003; Scott et al., 2003) or the enzymatic activity of FAP itself (Aertgeerts et al., 2005; LeBeau et al., 2009; Huang et al., 2011). The third line of research has been prompted by the recent observation that conditionally depleting FAP⁺ stromal cells from immunogenic, transplanted tumors in mice led to immune control of tumor growth (Kraman et al., 2010) and so is based on a biological role of the tumoral FAP⁺ stromal cell rather than on the FAP protein. Accordingly, the FAP⁺ stromal cell may be both a means by which cytotoxic drugs can be delivered to tumors for the purpose of killing cancer cells and a cytotoxic target itself for the purpose of alleviating tumoral immune suppression and promoting cancer immunosurveillance.

A contraindication to any potential cancer therapy that may indiscriminately deplete FAP⁺ cells, however, might be their presence in normal tissues. This consideration is raised by the finding of FAP⁺ stromal cells in two normal tissues of humans, the placenta and uterus (Dolzign et al., 2005), in the bone marrow of the adult mouse (Kraman et al., 2010), and in the somites of the mouse embryo (Niedermeyer et al., 2001). The full significance of this potential contraindication to the systemic depletion of FAP⁺ cells is not known, however, because there has not been a comprehensive analysis of occurrence and function of FAP⁺ stromal cells in normal tissues and organs.

We generated a transgenic mouse model that permits both the bioluminescent imaging of cells expressing FAP and their conditional ablation. The use of this model has demonstrated that FAP⁺ cells reside in almost all tissues of the adult mouse. In at least three of these, they share a common transcriptome, and in at least two, skeletal muscle and bone marrow, they have the essential functions of maintaining skeletal muscle mass and normal hematopoiesis, respectively. Remarkably, FAP⁺ stromal cells are altered in skeletal muscle and bone marrow in two mouse models of cancer-induced cachexia and anemia, two cancer comorbidities which severely reduce quality of life and contribute to fatal outcome. Therefore, FAP⁺ cells of normal tissues mediate essential physiological functions, and their alteration in cancer may contribute to two paraneoplastic syndromes.

RESULTS

FAP⁺ stromal cells are widely distributed in the adult mouse

A transgenic albino (Tyr^{-/-}) C57BL/6 mouse line was established with a bacterial artificial chromosome (BAC) containing

the *Fap* gene that had been modified by inserting at the start codon a cassette comprised of the coding sequences of firefly luciferase, the human diphtheria toxin (DTX) receptor (DTR), and mCherry that were linked by E2A sequences (Fig. 1 A; Szymczak et al., 2004). BAC transgenic mice were injected with D-luciferin and assessed for bioluminescence before and after DTX treatment for 3 d. The entire dorsal and ventral surfaces of the BAC transgenic mice were bioluminescent. Treatment with DTX to deplete the FAP⁺ stromal cells diminished the bioluminescent signal (Fig. 1 B). With the exception of lung, liver, and spleen, bioluminescence was observed in all organs that were examined in the BAC transgenic mouse and was sensitive to DTX treatment (Fig. 1 C and not depicted). FAP mRNA was also detected in these tissues (Fig. 1 D) at levels that correlated with those of luciferase, a marker of the expression of the BAC transgene (Fig. 1 E). FAP⁺ stromal cells were also identified by flow cytometric analysis of cells in enzyme-dispersed preparations of five of these tissues and organs (Fig. 1 F). These FAP⁺ stromal cells were sort purified, and mRNA for both FAP and luciferase were selectively found in the sorted FAP⁺ cells, indicating that the transgene accurately reports transcription of endogenous *Fap* (Fig. 1 G). FAP⁺ cells in transgenic mice also selectively showed a significantly increased mCherry mean fluorescence intensity compared with these cells in littermate controls, but the level was too low to be useful in detecting FAP expression.

FAP⁺ stromal cells may comprise a distinct cell lineage

FAP⁺ stromal cells from two mesenchymal tissues, visceral adipose tissue and skeletal muscle, and an epithelial organ, the pancreas, were selected for further analysis. FAP⁺ cells from these sources were analyzed by flow cytometry and found to uniformly express CD90, CD140a, and Sca-1 (Fig. 2 A). To further investigate whether these represented homogenous populations, these FAP⁺ cells and FAP⁻ MEFs were sort purified and their transcriptomes were assessed by RNA-Seq. The high quality of the RNA-Seq data was confirmed by mapping statistics and by high correlations between biological replicates (Table S1). To assess homogeneity of gene expression, expression levels were log transformed for both these cells and publically available data for CD4⁺ T-helper subsets (Wei et al., 2011). The degree to which this transformation conforms to a model bimodal distribution is a measure of the homogeneity of a cellular population. Genes below the cut off to be included in the highly expressed peak but above the cut off to be included in the lowly expressed peak were classified as intermediate genes (Hebenstreit et al., 2012). The percent of intermediate (%int) genes is a read out of conformity to the bimodal model, with lower numbers indicating greater homogeneity (Fig. 2 B; Hebenstreit et al., 2011). The %int values indicated that the FAP⁺ cells from these four organs and tissues were at least as homogeneous as were the four subsets of CD4⁺ T cells.

The similarity of the transcriptomes of the FAP⁺ cells was assessed by performing expression correlation, principal component analysis (PCA), clustering, and differential expression analyses. The transcriptomes of the FAP⁺ cells from the three tissues were highly correlated with each other and were distinct

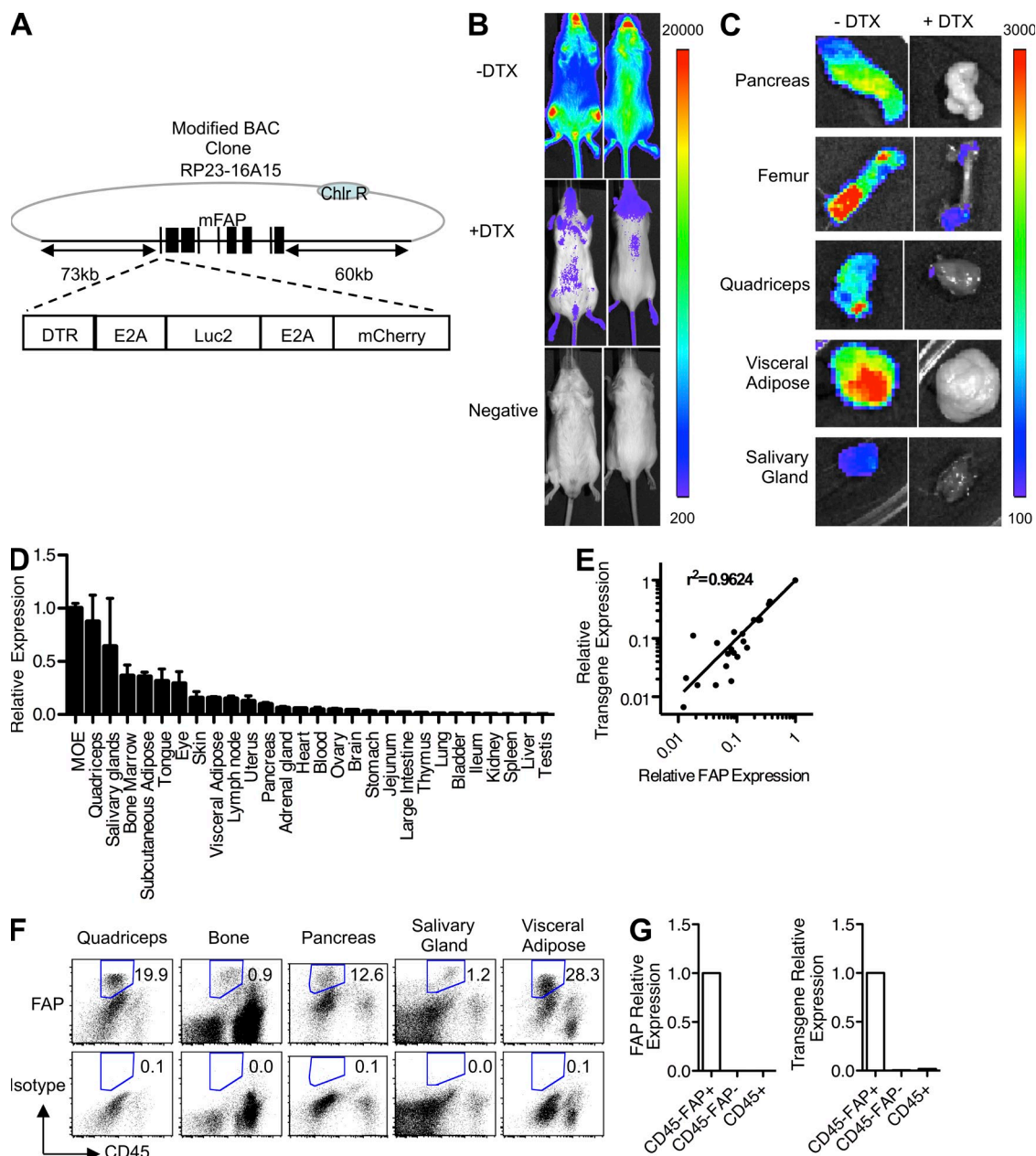


Figure 1. The tissue distribution of FAP⁺ stromal cells in the adult mouse. (A) A *Fap*-containing BAC was modified by inserting at the start codon a cassette encoding the DTR, Luc2, and mCherry linked by E2A sequences. (B) BAC transgenic mice in which luciferase and the DTR are expressed in FAP⁺ stromal cells and littermate mice were assayed for bioluminescence before and 24 h after two daily doses of 25 ng/g DTX. (C) Organs that had been dissected from DTX- or vehicle-treated BAC transgenic mice from B were assessed for bioluminescence. (B and C) The scale represents relative counts. (D) FAP mRNA levels were measured in different tissues by qRT-PCR. (E) FAP mRNA levels were correlated with those of luciferase, a marker of the expression of the BAC transgene, across different tissues by qRT-PCR. (F) Tissues were enzymatically dissociated, and cells were stained with antibodies to FAP and CD45 for analysis by flow cytometry. Numbers represent the percentage of live cells gated as FAP⁺. (G) CD45⁻FAP⁺, CD45⁻FAP⁻, and CD45⁺ cells were sort purified from skeletal muscle and assessed by qRT-PCR for FAP and luciferase/transgene mRNA. Error bars represent SEM. MOE, main olfactory epithelium. Data are representative of more than three independent analyses ($n \geq 3$; B–G).

from that of FAP⁻ MEFs (Fig. 2 C). Previously published RNA-Seq data on CD4⁺ T cell subsets, which were used as the outgroup (Wei et al., 2011), showed these cells also to be distinct from FAP⁺ cells and FAP⁻ MEFs (Fig. 2 C). These relationships were observed using both Pearson and Spearman

correlations and on both reads per kilobase million (RPKM) and bias-adjusted fragments per kilobase million (FPKM) values (not depicted). PCA demonstrated that FAP⁺ stromal cells from these sites formed a discrete cluster that was distinct from that of the CD4⁺ T cells and from the FAP⁻ MEFs

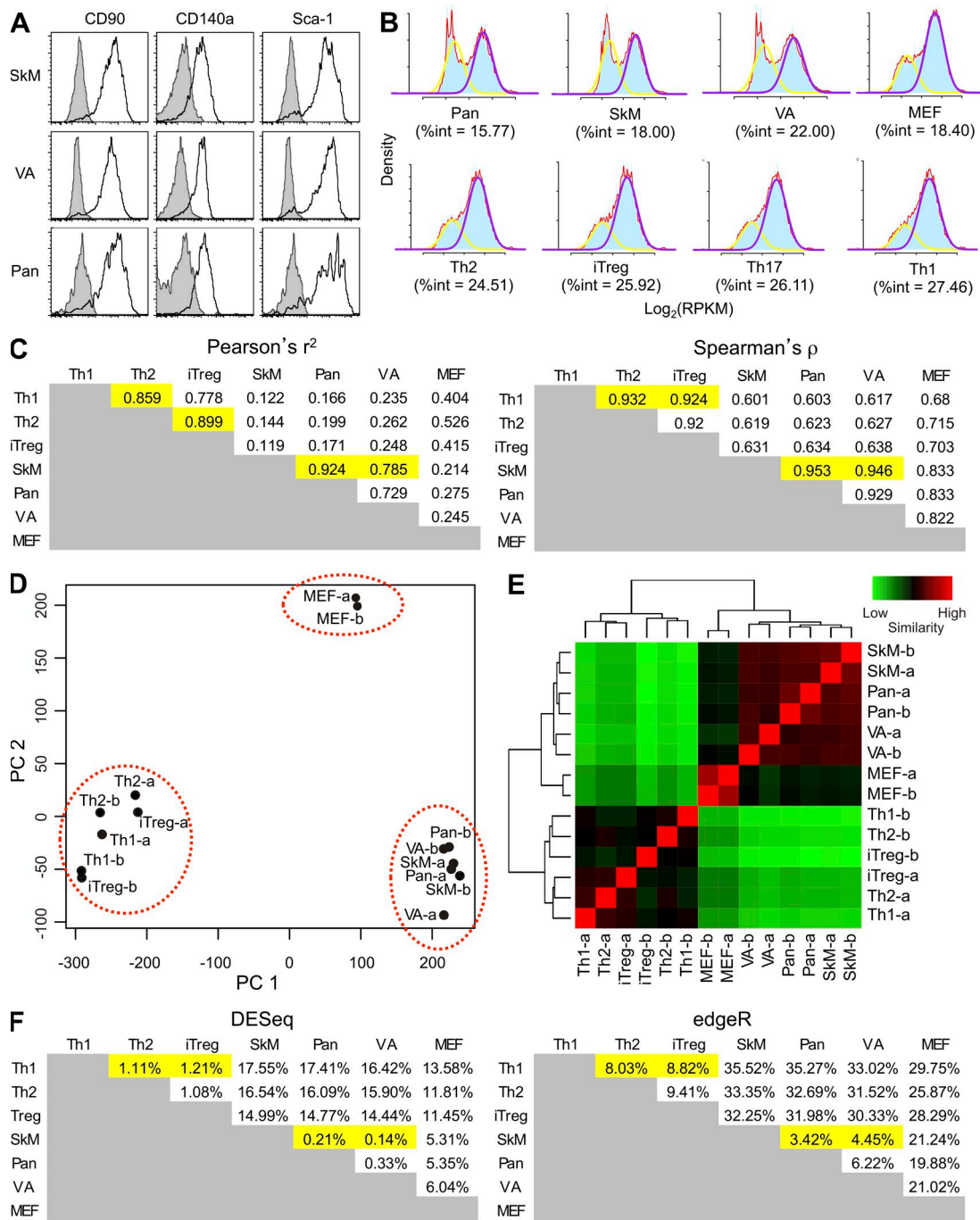


Figure 2. Analysis of the transcriptomes of FAP⁺ cells from adipose tissue, skeletal muscle, and pancreas. (A) FAP⁺ cells were assessed by flow cytometry for their expression of the membrane proteins CD90 (Thy1), CD140a (PDGFR α), and Sca-1 (Ly6A/E), which are characteristic of certain mesenchymal cells. Filled histograms represent isotype staining, and the black lines denote the specific stains. (B) The RNA-Seq data for each of the cell types were log transformed and modeled as bimodal distributions. The %int represents the degree of heterogeneity within each population. The density value is indicated in blue. The yellow line represents the bimodal fit for the lowly expressed transcripts and the purple line for the highly expressed transcripts, and the red line indicates the overall density value. (C) The Pearson's r^2 and Spearman's ρ correlations were calculated for the RPKM gene expression levels of FAP⁺ cells, FAP⁻ MEFs, and CD4⁺ T cell subsets after removal of low expressed/nonexpressed genes. (D) PCA analysis of VST (counts) of FAP⁺ cells, CD4⁺ T cell subsets, and MEFs is shown. (E) VST clustering of RPKM levels of replicate samples of FAP⁺ cells, CD4⁺ T cell subsets, and MEFs is shown. (F) The percentage of differentially expressed genes among the different cells was determined by DESeq and edgeR using count data. The highlighted cells here and in C show the correspondence between high levels of similarity in these two analyses of gene expression. Th1, Th2, and iTreg refer to the CD4⁺ T cell subsets. VA, SkM, and Pan refer to FAP⁺ cells from visceral adipose tissue, skeletal muscle, and pancreas, respectively. See also Table S1.

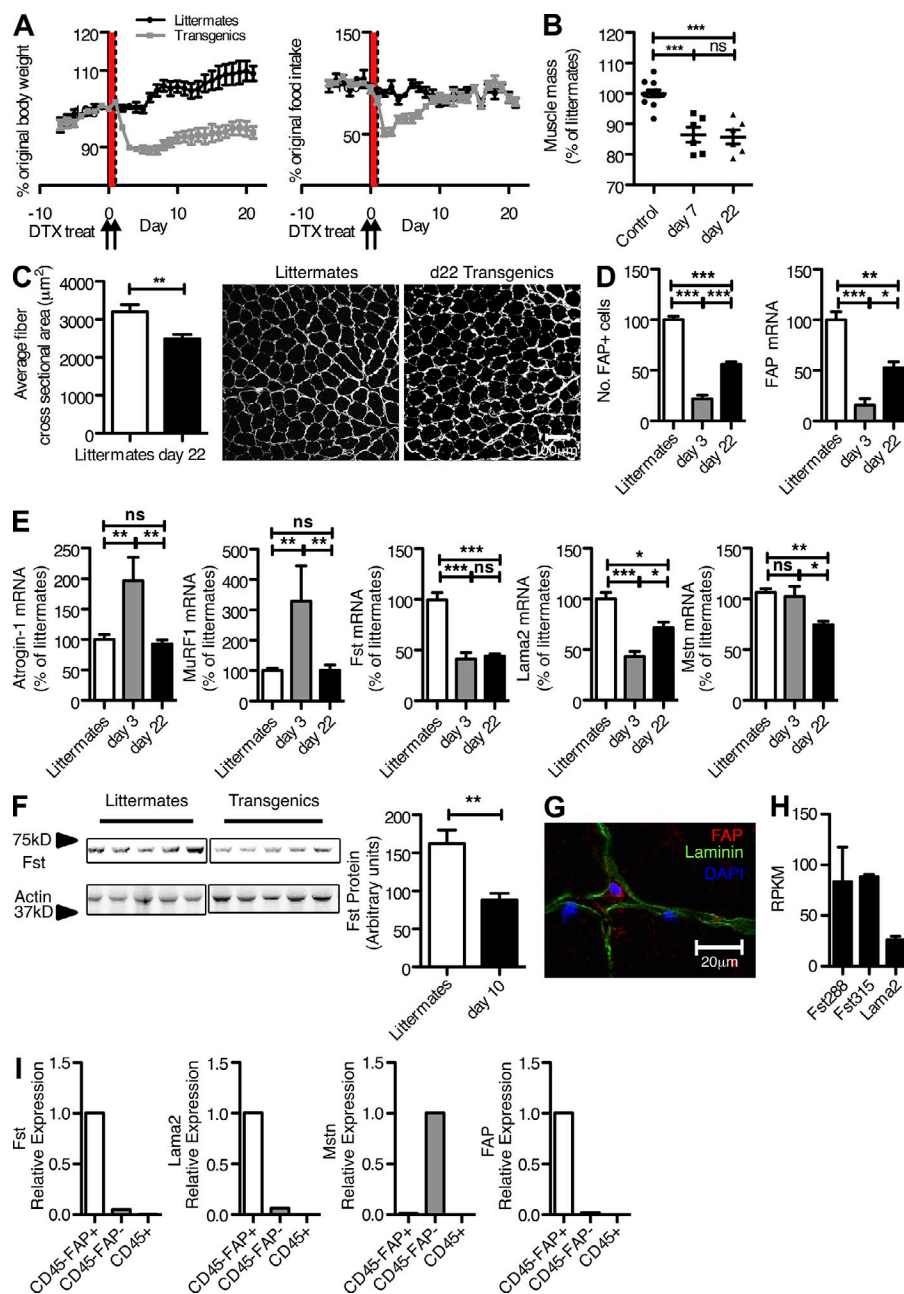


Figure 3. Depletion of FAP⁺ stromal cells and loss of skeletal muscle mass. (A) BAC transgenic mice and littermates were treated with DTX for 2 d, and total body weight and food intake were measured each day during the ensuing 3 wk. Arrows indicate when DTX was given, and the red highlighting shows the period over which it was being administered. (B) The mass of the quadriceps muscles from BAC transgenic mice and littermates was measured on days 3 and 22 after DTX treatment. (C) The mean cross-sectional area of the fibers of the quadriceps muscles from BAC transgenic mice and littermates taken 22 d after DTX treatment was measured, after fibers were delineated by staining with antibody to the basal lamina. Bar, 100 μm . (D) The number of FAP⁺ cells and the level of FAP mRNA in quadriceps muscles of BAC transgenic mice as a percentage of littermates were measured 3 and 22 d after DTX treatment. (E) The mRNA levels for atrogen-1, MuRF1, Fst, Lama2, and Mstn in quadriceps muscles of BAC transgenic mice and littermates were measured 3 and 22 d after DTX treatment. (F) The levels of Fst protein in quadriceps muscles of BAC transgenic mice and littermates were measured by immunoblot analysis 10 d after DTX treatment. (G) Quadriceps muscle from a normal mouse was stained with antibodies to FAP and laminin and assessed by confocal microscopy. (H) The FAP⁺ subset of enzymatically dissociated cells from quadriceps muscle were sort purified, and the mRNA levels of Lama2, Fst288, and Fst315 in FAP⁺ cells were determined by RNA-Seq. (I) The indicated subsets of enzymatically dissociated cells from quadriceps muscle were sort purified, and the mRNA levels of Fst, Lama2, Mstn, and FAP were determined by qRT-PCR. Error bars represent SEM. *, $P < 0.05$; **, $P < 0.01$; ***, $P < 0.001$. Data are representative of more than three independent analyses ($n \geq 3$; A) or representative of two independent analyses ($n \geq 5$; B-F).

(Fig. 2 D). These groupings were observed with PCA when variance-stabilized transform (VST) counts or VST fragments (not depicted) were used. Cluster analysis confirmed the similarity of the FAP⁺ stromal cells from the three tissues and suggested that, as anticipated, they were more related to FAP⁻ MEFs than to the subsets of CD4⁺ T cells (Fig. 2 E). This same pattern of clustering was seen using both VST counts and fragments and using hierarchical clustering with different distance metrics on RPKM data for the whole transcriptome or just transcription factors (not depicted). Finally, differential gene expression analysis showed that few genes were differentially expressed when the FAP⁺ cells from the three tissues were compared, whereas there were many more differentially expressed genes relative to

FAP⁻ MEFs and the CD4⁺ T cell subsets (Fig. 2 F). This was observed whether considering counts or fragments using both DESeq and edgeR (not depicted). From these various analyses, it can be concluded that the FAP⁺ stromal cells from adipose tissue, skeletal muscle, and pancreas consistently appear to be as similar to each other as are members of the CD4⁺ T cell lineage, supporting the possibility that they may be members of a developmentally distinct cell lineage.

Depleting FAP⁺ stromal cells from skeletal muscle causes an atrophic muscle response

In this first examination of the biological consequences of the loss of FAP⁺ stromal cells, we limited our analysis to obvious

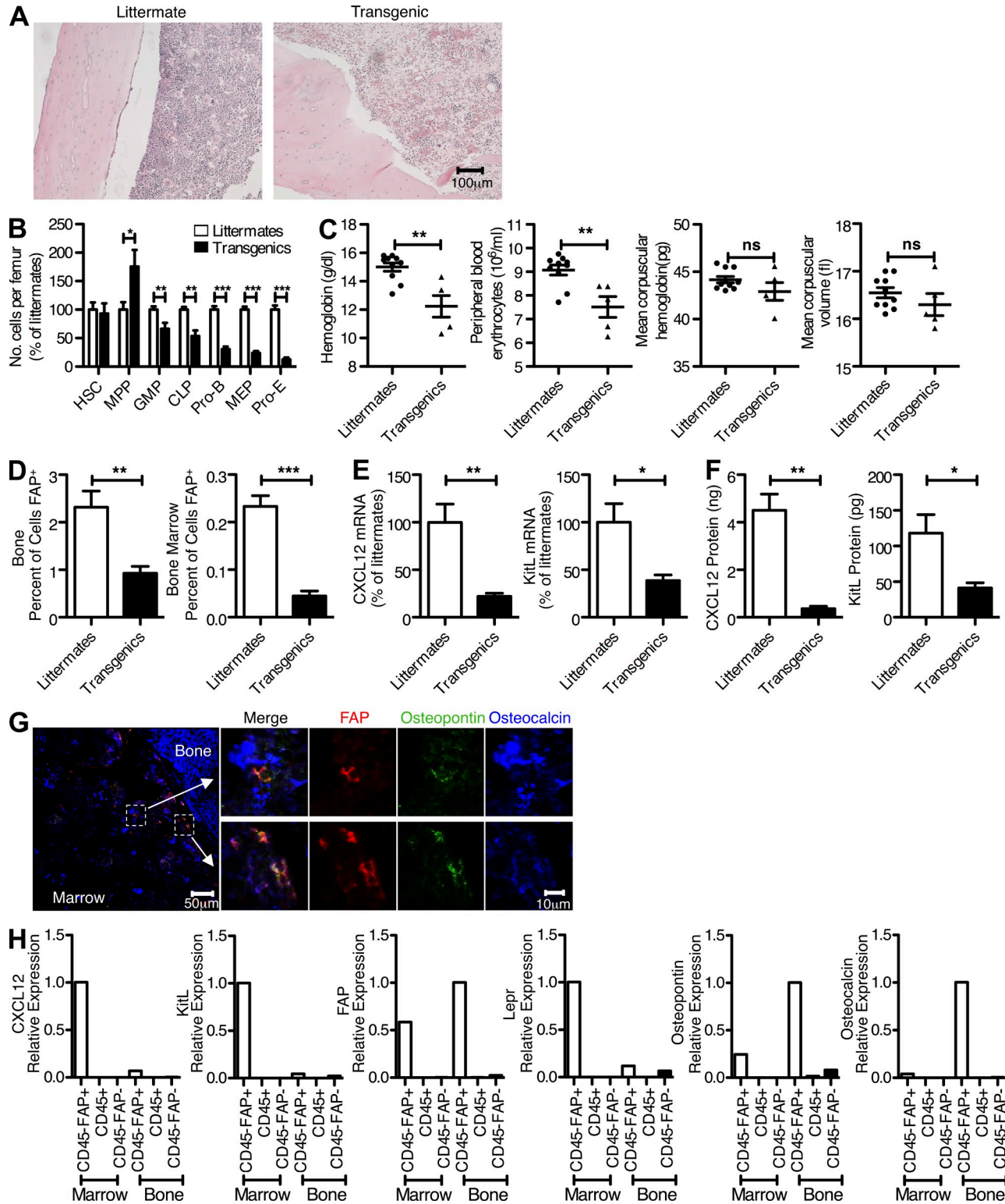


Figure 4. FAP⁺ cells of the bone marrow and hematopoiesis. (A) The cellularity of the femoral bone marrow from BAC transgenic mice and littermates was determined by hematoxylin and eosin staining after 3-d treatment with DTX. (B) Individual populations of hematopoietic cells from the femoral bone marrow of BAC transgenic mice and littermates were analyzed by flow cytometry after 3-d treatment of the mice with DTX. (C) 7 d after DTX administration, samples of peripheral blood from transgenic and littermate mice were assayed for hemoglobin, erythrocyte numbers, mean corpuscular hemoglobin, and mean corpuscular volume. (D) The proportions of FAP⁺ cells in enzyme-dissociated bone and bone marrow preparations from BAC transgenic mice and littermates were assessed by flow cytometry after 3-d treatment of the mice with DTX. (E) The mRNA levels of Cxcl12

changes occurring soon after DTX administration. Although mice depleted of FAP⁺ cells did not exhibit any reduction in activity or other signs of distress, there were two conspicuous changes affecting fundamental physiological processes: rapid weight loss (Fig. 3 A) and altered hematopoiesis, as manifested by hypocellularity of the bone marrow (Fig. 4 A). The former was accompanied initially by decreased food intake, but normal food intake resumed by 10 d after DTX without a corresponding recovery in weight, excluding the transient alteration in food intake as an explanation for the persistent loss of total body weight (Kennedy, 1950). There was a significant reduction in muscle mass as seen by direct measurement of the quadriceps taken 7 and 22 d after DTX treatment, and measurement of a myofiber cross-sectional area 22 d after DTX revealed a significant decrease (Fig. 3, B and C), indicating atrophy rather than loss of myocytes. Therefore, depletion of FAP⁺ stromal cells causes cachexia, which is a reduction in muscle mass despite adequate food intake (Evans et al., 2008).

Serum was taken on day 12 after DTX and assessed for changes that would reflect a basic metabolic change that could explain the persistent weight loss (Table 1). Compared with the littermate controls, DTX-treated mice had a tendency toward elevated serum alanine aminotransferase levels. Because there were no other abnormal liver function tests, this finding is likely to reflect the skeletal muscle catabolism that was occurring in these mice. Serum insulin and glucose levels were normal, excluding a pancreatic endocrine dysfunction. Renal insufficiency was ruled out with the normal urea nitrogen levels, and albumin and total protein concentrations were also normal. Finally, fecal energy, as determined by bomb calorimetry, was the same in DTX-treated and littermate controls, which indicated that weight loss was not caused by intestinal malabsorption.

Having excluded a generalized metabolic disorder resulting from the depletion of FAP⁺ cells as the basis for the DTX-induced cachexia, an abnormality caused by the loss of FAP⁺ stromal cells from skeletal muscle itself (Fig. 1 C) that directly affected this tissue was sought. The loss of skeletal muscle mass (Fig. 3 B) was associated with a decrease in the mean cross-sectional area of the myofibers (Fig. 3 C). A persistent loss of FAP⁺ cells caused by DTX treatment was confirmed by measurement of FAP mRNA and of the number of FAP⁺ cells in the quadriceps (Fig. 3 D). Muscle wasting in the mouse may be secondary to increased signaling through the type II activin receptor (AcvRIIB), which may be caused by an imbalance between the levels of the TGF- β family members, myostatin

(Mstn) and activin A, and follistatin (Fst), an inhibitor of their binding to the AcvRIIB (McPherron and Lee, 1997; Lee and McPherron, 2001; Zimmers et al., 2002). The AcvRIIB signals Foxo-dependent expression of the myocyte-specific E3 ubiquitin ligases, muscle atrophy F-box/atrogin-1, and muscle RING finger protein/MuRF1 (Bodine et al., 2001; Gomes et al., 2001; Glass, 2010), which ubiquitinate muscle-specific proteins and promote their proteasomal degradation (Bodine et al., 2001; Gomes et al., 2001; Lee et al., 2005; McFarlane et al., 2006). Muscle wasting may also be caused by abnormalities of the β -dystroglycan complex and laminin α 2 (Lama2) of the basal lamina, which induce the expression of atrogin-1 and MuRF1 (Carmignac et al., 2011).

The depletion of FAP⁺ stromal cells affects both pathways of muscle atrophy by causing an acute and persistent decrease of Fst and Lama2 mRNA levels at days 3 and 22. These changes led to a transient increase in atrogin-1 and MuRF1 mRNA levels at day 3, which did not persist at day 22, perhaps because of a compensatory decrease of the Mstn mRNA level (Fig. 3 E). Fst protein in the quadriceps muscle also was decreased, confirming the finding of the reduced Fst mRNA levels (Fig. 3 F). Similar changes were seen in the gastrocnemius muscle that persisted at least until day 90 after DTX (not depicted).

We examined the skeletal muscle FAP⁺ stromal cell to determine whether its depletion was directly responsible for these changes. Confocal microscopy showed these cells to be located outside the basal lamina of the myofibers, distinguishing them from satellite cells that reside inside the basal lamina (Fig. 3 G; Mauro, 1961). RNA-Seq analysis of the sort-purified FAP⁺ stromal cells demonstrated transcription of the genes encoding Lama2 and both the Fst288 and Fst315 isoforms (Fig. 3 H). Analysis by quantitative RT-PCR (qRT-PCR) of mRNA from sorted skeletal muscle cells revealed that FAP⁺ stromal cells were the major source of both Fst and Lama2 and that FAP⁻/CD45⁻ cells, presumably mainly myocytes, were the source of Mstn (Fig. 3 I). FAP expression was limited to the FAP⁺ population and CD3 to the CD45⁺ cells, confirming the sort purity (Fig. 3 I). Therefore, the depletion of skeletal muscle FAP⁺ stromal cells was directly responsible for the loss of Fst and Lama2 in this tissue, which may reasonably be considered to be the basis of the acute increase of atrogin-1 and MuRF1 (Gomes et al., 2001). DTX-induced weight loss in the BAC transgenic mice was not associated with an increase in the plasma levels of corticosterone, IL-6, or TNF (not depicted), all of which have been reported to cause loss of muscle mass. We do not have an explanation for the transient

and KitL in cells of the femoral bone marrow from BAC transgenic mice and littermates were measured by qRT-PCR after 3-d treatment of the mice with DTX. (F) The protein levels of Cxcl12 and KitL in lysates of bone marrow from BAC transgenic mice and littermates were measured by ELISA after 3-d treatment of the mice with DTX. (G) A cross-section of normal mouse femur was stained with antibodies to FAP, osteopontin, and osteocalcin and assessed by confocal microscopy. (H) Subsets of enzymatically dispersed cells from femoral bone and marrow were FACS purified, and the sorted populations were assessed by qRT-PCR for expression of FAP, Cxcl12, KitL, osteopontin, osteocalcin, and Lepr. Error bars represent SEM. *, $P < 0.05$; **, $P < 0.01$; ***, $P < 0.001$. Data are representative of at least two independent analyses ($n \geq 4$; A, B, D, and E) or one confirmatory analysis ($n = 6$; F). Combined data are from three independent experiments ($n \geq 4$; B).

Table 1. Analyses of plasma and feces from transgenic and littermate mice 12 d after DTX administration

Parameter	Littermates	Transgenics	P-value	Normal range
Gamma glutamyl peptidase (U/liter)	0.2 ± 0.2	0.0 ± 0.0	0.35	0.0–0.2
Aspartate aminotransferase (U/liter)	150.0 ± 45.1	167.2 ± 28.2	0.75	59–247
Alanine aminotransferase (U/liter)	24.4 ± 3.1	114.6 ± 51.3	0.12	28–132
Urea nitrogen (mmol/liter)	7.2 ± 0.5	6.1 ± 0.6	0.79	6.4–10.4
Glucose (mmol/liter)	15.0 ± 0.2	14.1 ± 0.8	0.38	9.0–19.3
Insulin (µg/liter)	0.3 ± 0.1	0.3 ± 0.1	0.61	0.1–2.9
Albumin (g/liter)	27.6 ± 2.0	26.6 ± 1.2	0.68	25–48
Bilirubin (µmol/liter)	6.4 ± 0.9	6.0 ± 1.0	0.78	2–15
Total protein (g/liter)	51.0 ± 2.3	52.2 ± 0.6	0.62	36–66
Phosphate (mmol/liter)	2.1 ± 0.1	2.6 ± 0.2	0.10	1.97–3.26
Calcium (mmol/liter)	2.0 ± 0.1	1.9 ± 0.1	0.26	1.47–2.35
Fecal energy (kJ/g)	13.7 ± 0.7	13.7 ± 0.5	0.98	

Data are representative of two independent analyses and are expressed as mean ± SEM ($n \geq 5$). Fecal energy does not have a well-established normal range as it differs depending on chow so much. As a result, we have simply compared with littermate controls as these were fed at the same time with the same chow.

reduction in food intake, as an analysis of hypothalamic tissue (Coll et al., 2007) revealed increased expression of the orexigenic peptides *NPY* and *AgRP* in DTX-treated BAC transgenic mice (not depicted).

Depleting FAP⁺ cells from the bone marrow suppresses erythropoiesis and B lymphopoiesis

The acute hypocellularity of the bone marrow (Fig. 4 A) seen 3 d after DTX treatment of BAC transgenic mice reflected a marked decrease in the subpopulations of megakaryocyte-erythroid progenitors (MEPs: Lin⁻, c-Kit⁺, Sca-1⁻, CD16/32⁻, CD34⁻), proerythroblasts (pro-Es: c-Kit⁺, CD71⁺, Ter119^{int}), and pro-B cells (pro-Bs: CD19⁺, IgM⁻, c-Kit⁺) and modest losses of the common lymphoid progenitors (CLPs: Lin⁻, CD135⁺, CD127⁺) and granulocyte-macrophage progenitors (Lin⁻, c-Kit⁺, Sca-1⁻, CD16/32⁺, CD34⁺; Fig. 4 B). The multipotent progenitors (Lin⁻, c-Kit⁺, Sca-1⁺, CD135⁺) were slightly enriched, and there was no change in the hematopoietic stem cells (HSCs: Lin⁻, c-Kit⁺, Sca-1⁺, CD150⁺, CD48⁻, CD34⁻; Omatsu et al., 2010). Peripheral blood taken 7 d after DTX treatment showed that these mice had a normocytic, normochromic anemia with reduced erythrocyte number and hemoglobin but normal mean corpuscular volume and hemoglobin (Fig. 4 C). The decreased femoral bioluminescence (Fig. 1 C) in the DTX-treated mouse was caused by loss of FAP⁺ stromal cells from both bone and bone marrow (Fig. 4 D). This loss was associated with decreased expression of two contributors to hematopoiesis, Cxcl12 and KitL, at both the transcript and protein levels (Fig. 4, E and F).

Confocal microscopy of bone revealed the presence of two types of FAP⁺ cells: those showing triple staining for FAP, osteocalcin, and osteopontin, which have a characteristic cuboidal aspect and line the bone endosteum, and those that are deeper in the marrow and are positive for osteopontin but not osteocalcin (Fig. 4 G). These anatomically distinct FAP⁺ stromal cells also differed with respect to their potential roles in the hematopoietic phenotype in that FAP⁺ cells that had been

FACS sorted from pooled bone marrow cells of six donors, but not those from bone, expressed Cxcl12 and KitL (Fig. 4 H). In keeping with the confocal microscopy, only FAP⁺ cells isolated from bone expressed osteocalcin (Fig. 4 H). The finding that the bone marrow-derived FAP⁺ stromal cell expresses Cxcl12 and KitL and has an essential role in erythropoiesis and B lymphopoiesis is consistent with at least some of this population being comprised of the CAR (Cxcl12-abundant reticular) cell (Omatsu et al., 2010). The additional finding that the FAP⁺ cells from the bone marrow expressed the leptin receptor (Lepr; Fig. 4 H) identifies them as a component of the HSC niche (Ding et al., 2012). Endothelial cells may have not been present in the FACS-sorted FAP⁻/CD45⁻ cells from the bone marrow, thus accounting for the absence of detectable mRNA for KitL and Lepr in this population.

Cancer-induced cachexia and anemia and alteration of FAP⁺ stromal cells in skeletal muscle and bone marrow

Patients with cancer suffer not only from direct consequences of tumors, but also from indirect, paraneoplastic effects, two of which are cachexia and anemia. It has been difficult to understand how cancers alter the function of two such disparate organ systems as skeletal muscle and the bone marrow because they had not been known to share a biologically relevant cell type. The present finding of the essential roles of the FAP⁺ stromal cell in skeletal muscle metabolism and erythropoiesis made it a candidate for the shared entity that may be affected by cancer to cause cachexia and anemia.

To examine the possibility that alterations of the FAP⁺ stromal cell may contribute to cancer cachexia and anemia, C26 colon carcinoma cells were implanted subcutaneously in BAC transgenic C57BL/6 × BALB/c F1 mice (Tanaka et al., 1990). Within 3–4 wk, the mice suddenly lost weight, despite their food intake being comparable with nontumor-bearing littermates (Fig. 5 A), and the level of whole body, FAP-dependent bioluminescence became diminished at the time that the mice began to lose weight (Fig. 5 B). The dissected

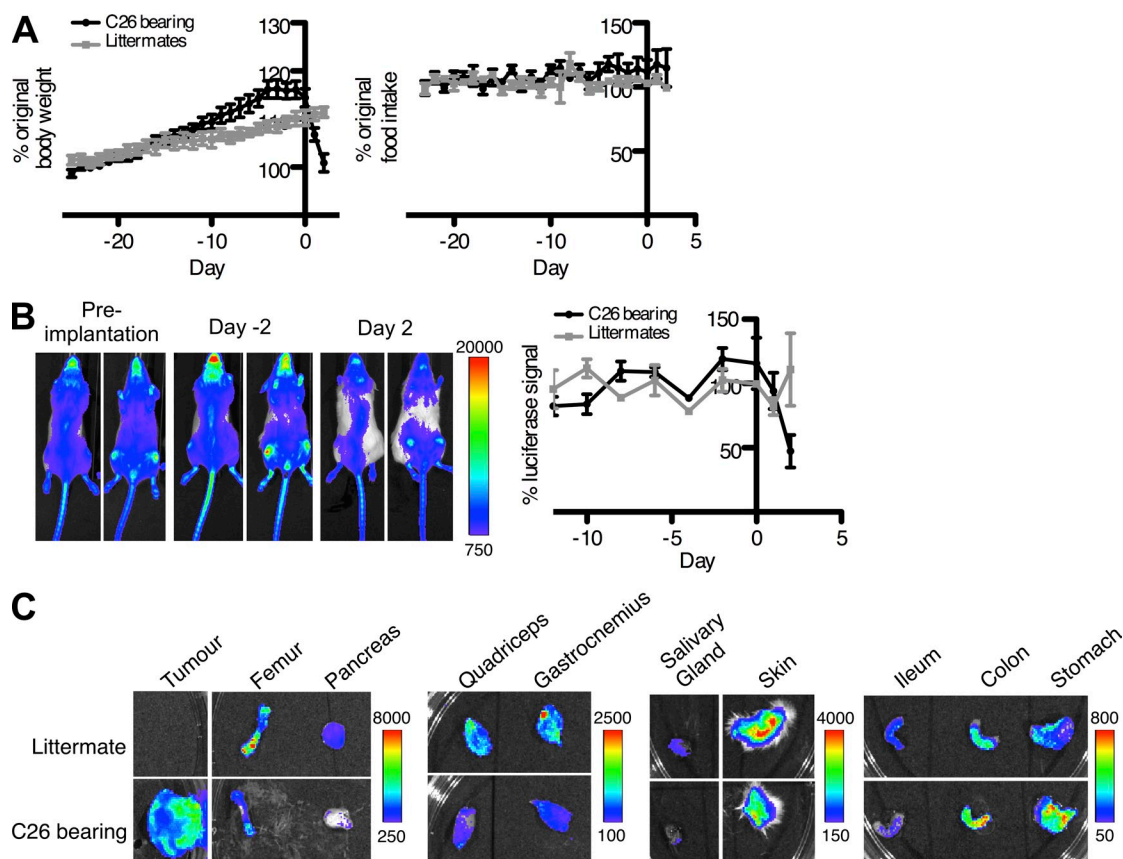


Figure 5. The transplanted C26 carcinoma, cachexia, and systemic alterations in FAP⁺ stromal cells. (A) Whole body weight and food intake of C57BL/6 × BALB/c F1 mice with and without ectopic C26 tumors were measured during the 3–4-wk post-tumor implantation period. (B) C26 cells were subcutaneously inoculated into BAC transgenic C57BL/6 × BALB/c F1 mice. Whole body bioluminescence was quantified for the entire dorsal surface of the mice at the indicated times. (C) The levels of bioluminescence of the excised C26 tumor and several tissues of tumor-bearing mice and littermate controls were assessed. (B and C) Scale represents relative counts. Error bars represent SEM. Data are representative of three independent analyses ($n = 4$ for A and B; representative $n = 1$ for C).

tumors (2.5 ± 0.1 g, mean \pm SEM) were bioluminescent (Fig. 5 C), indicating an accumulation of FAP⁺ stromal cells at this site, which contrasted with the diminished bioluminescence of six of the dissected tissues: femur, pancreas, salivary gland, skin, and the quadriceps and gastrocnemius muscles (Fig. 5 C). The small intestine also appeared to have diminished bioluminescence, whereas the stomach and colon had increased bioluminescent signals.

The reduction in quadriceps muscle mass (Fig. 6 A) confirmed the occurrence of cachexia. The diminished bioluminescence of this tissue was caused by decreased expression of the endogenous *Fap* gene, which, importantly, was associated with a reduction in two products of the FAP⁺ stromal cell, Fst, measured both as mRNA and protein, and Lama2 (Fig. 6, B and C). These changes were accompanied by elevated expression of atrogin-1 and MuRF1, presumably reflecting increased signaling through the AcvRIIB secondary to the decreased Fst and Lama2, and by a twofold increase in skeletal muscle Mstn (Fig. 6 B), which occurs with cachexia in this tumor model (Zhou et al., 2010). The same findings were observed in the gastrocnemius (not depicted).

The femoral marrow of C26-bearing mice also showed a significant loss of FAP⁺ cells (Fig. 6 D), confirming the bioluminescence findings (Fig. 5 C). FACS analysis of the bone marrow cells revealed depletion of the MEP, pro-E, pro-B, and CLP populations (Fig. 6 D), mirroring the effects of DTX-mediated depletion of the FAP⁺ cell (Fig. 4 B). This loss of FAP⁺ cells was associated with a decrease in expression of both *Cxcl12* and *KitL* from the bone marrow (Fig. 6 E).

Cachexia frequently develops in patients with pancreatic ductal adenocarcinoma (PDA; Tisdale, 2009). A genetically engineered mouse model of this disease, the KPC (*Kras*^{G12D/+}; *Trp53*^{R172H/+}; *Pdx-1* Cre) mouse in which the Cre-induced expression of the oncogenic *Kras*^{G12D} and *Trp53*^{R172H} alleles is directed specifically to pancreatic progenitor cells, has been shown to recapitulate the major histopathological, genomic, and clinical characteristics of human PDA (Hingorani et al., 2005). This autochthonous cancer model offered an opportunity to determine whether in these mice that became cachectic, there were similar abnormalities of FAP⁺ stromal cells. In PDA-bearing KPC mice that appeared on gross inspection to be

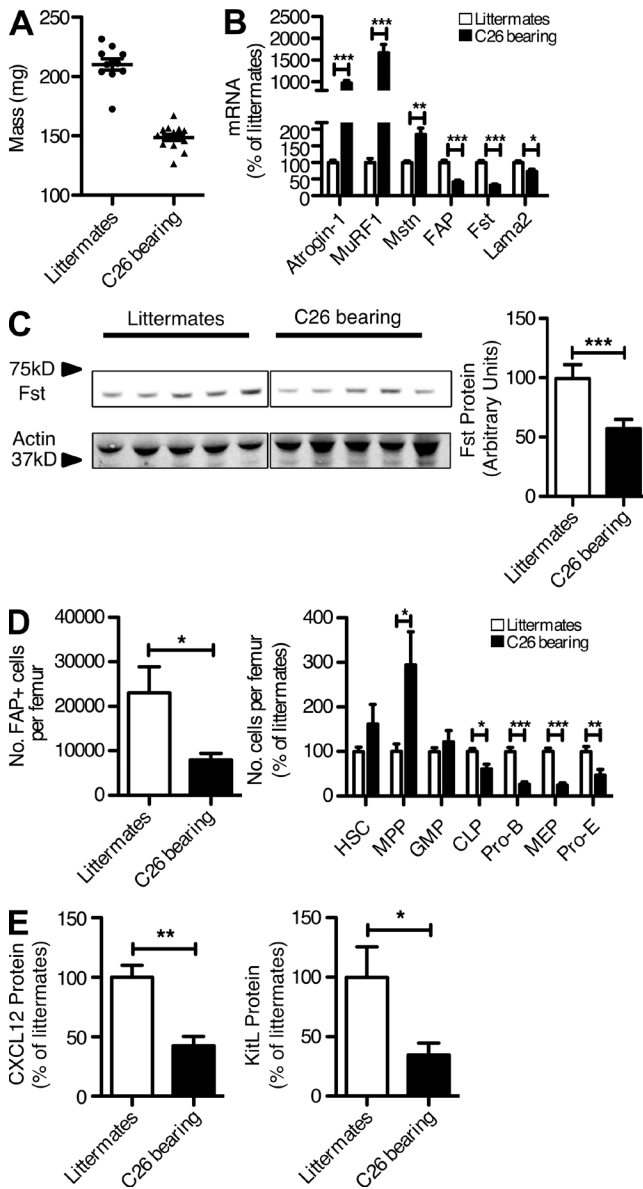


Figure 6. Alterations of FAP⁺ cells in the quadriceps muscle and bone marrow of cachectic mice bearing C26 tumors. (A and B) The quadriceps muscles from cachectic, C26-bearing and nontumor-bearing littermates were assessed for mass (A) and the mRNA levels of atrogin-1, MuRF1, Mstn, FAP, Fst, and Lama2 (B). (C) The levels of Fst protein in lysates of quadriceps muscles from cachectic, C26-bearing and nontumor-bearing littermates were measured by immunoblot analysis. (D) Individual populations of hematopoietic cells from the femoral bone marrow of cachectic, C26-bearing and nontumor-bearing littermates were assessed by flow cytometry. (E) The levels of Cxcl12 and KitL protein in lysates of cells recovered from the femoral bone marrow of cachectic, C26-bearing and nontumor-bearing littermates were measured by ELISA. Error bars represent SEM. *, $P < 0.05$; **, $P < 0.01$; ***, $P < 0.001$. Combined data are from three independent analyses ($n = 1-5$).

cachectic, examination of the quadriceps muscles revealed significant decreases in mass (Fig. 7 A) and increases in the mRNA levels of atrogin-1 and MuRF1 (Fig. 7 B) as compared

with PDA-bearing noncachectic KPC mice and nontumor-bearing littermate mice. This was accompanied by decreases in FAP, Fst, and Lama2 mRNA levels (Fig. 7 B). Mstn mRNA levels in the quadriceps muscle were not increased. All tumor-bearing KPC mice, including noncachectic mice, also displayed a normocytic, normochromic anemia that is consistent with the type of anemia commonly observed in cancer patients (Fig. 7 C). In these PDA-bearing mice, there were significant decreases in the relative number of FAP⁺ cells that could be recovered from the bone marrow, as well as in the relative numbers of MEPs, pro-Es, pro-Bs, and CLPs (Fig. 7 D). The reduction in FAP⁺ cells from the femur was accompanied by a loss of both Cxcl12 and KitL (Fig. 7 E). Therefore, cachexia and anemia in the KPC model of PDA is associated with an abnormality of FAP⁺ stromal cells in skeletal muscle and bone marrow. We have not excluded the possibility that cancer-induced abnormalities of FAP⁺ cells in other tissues may also cause physiological changes, as suggested by the systemic alteration in FAP-dependent bioluminescence in C26-bearing mice (Fig. 5, B and C) and by the finding of decreased levels of FAP mRNA in the heart and salivary gland of cachectic KPC mice (Fig. 7 F).

DISCUSSION

Before the present study, studies of FAP⁺ stromal cells had emphasized their occurrence in tumors and a range of chronic inflammatory conditions, with little attention being given to their presence in normal tissues (Rettig et al., 1986; Garin-Chesa et al., 1990; Levy et al., 1999; Bauer et al., 2006; Brokopp et al., 2011). Therefore, we were surprised to find that FAP⁺ stromal cells are present in the majority of normal tissues and organs, raising the possibility that FAP expression may identify a stromal cell lineage with biological roles that extend beyond those associated with wound healing (Fig. 1). Three experimental challenges were presented by this finding: determining whether the expression of FAP is indicative of a stromal cell lineage, elucidating the functions of FAP⁺ stromal cells in normal tissues, and seeking abnormalities of these cells that may contribute to disease.

FAP⁺ cells from two mesenchymal organs, visceral adipose and skeletal muscle, and an epithelial organ, the pancreas, showed highly similar transcriptomic profiles. The degree to which these correlated was similar to that of the CD4⁺ T cell subsets, known members of a common lineage (Fig. 2 C). The FAP⁺ cells from these three sites also had very few differentially expressed genes (Fig. 2 F), and this similarity cannot be ascribed to their sharing a common fibroblast gene expression profile, which, for the purpose of this study, was defined by the FAP⁻MEF transcriptome (Fig. 2, C and D). Fibroblasts have been shown to be diverse when isolated from different sites (Chang et al., 2002), whereas the FAP⁺ cells isolated from three different tissues are very similar. Thus, FAP⁺ cells may represent a distinct subset of mesenchymal cells, but more definitive studies are required to establish this relationship.

The presence in the BAC luciferase transgene of the cassette encoding the DTR afforded an opportunity for a

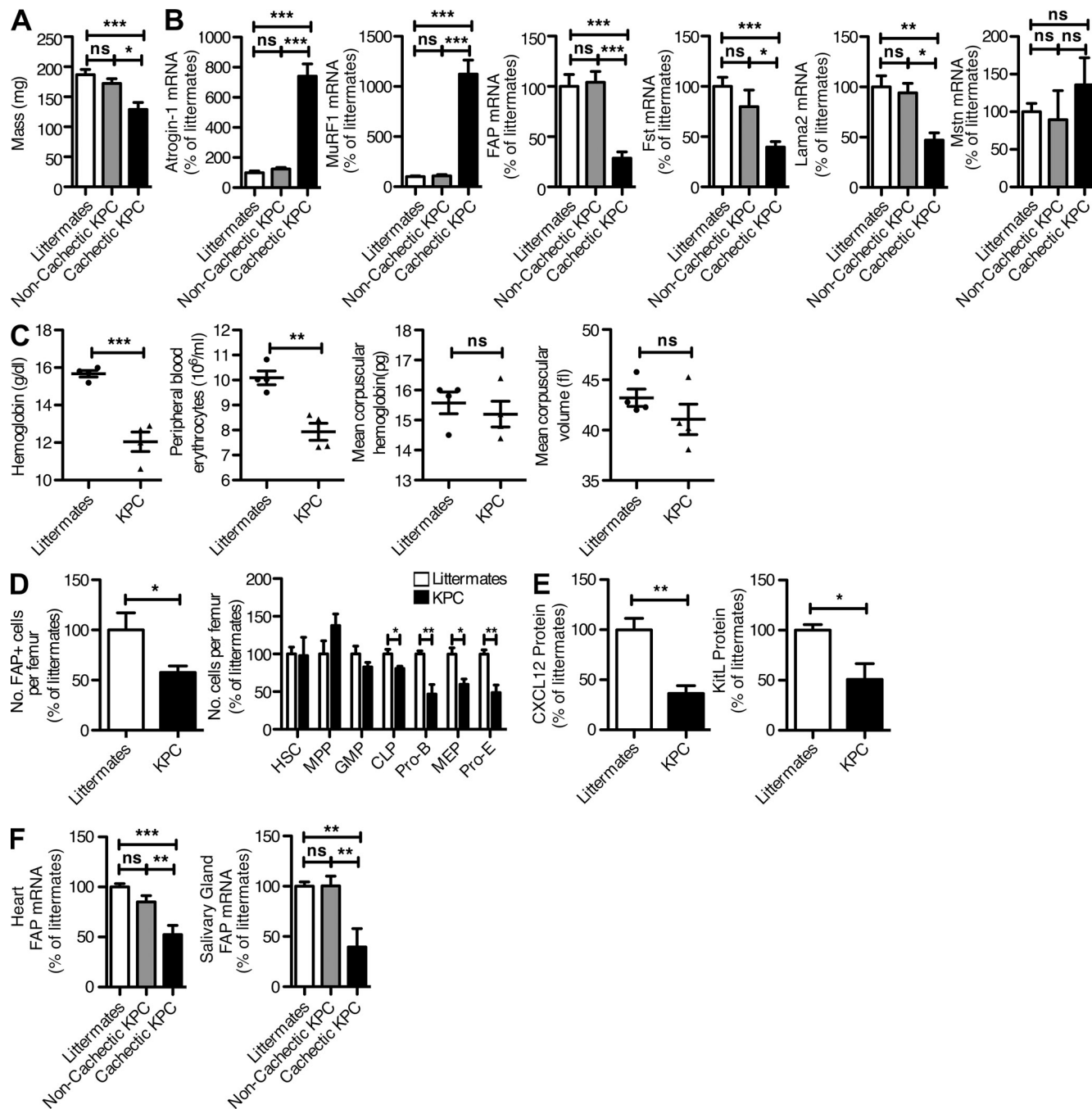


Figure 7. Alterations of FAP⁺ cells in the quadriceps muscle and bone marrow of KPC mice with PDA. (A and B) The quadriceps muscles from PDA-bearing KPC mice with and without cachexia and littermates were assessed for mass (A) and the mRNA levels of atrogin-1, MuRF1, FAP, Fst, Lama2, and Mstn (B). (C) Peripheral blood from PDA-bearing mice and nontumor-bearing littermates was assayed for hemoglobin, erythrocyte number, mean corpuscular hemoglobin, and mean corpuscular volume. (D) Individual populations of hematopoietic cells from the femoral bone marrow of PDA-bearing mice and nontumor-bearing littermates were assessed by flow cytometry. (E) The levels of CXCL12 and KitL protein in lysates of cells recovered from the femoral bone marrow of PDA-bearing KPC mice and nontumor-bearing littermates were measured by ELISA. (F) The mRNA levels of FAP in heart and salivary glands from KPC, PDA-bearing mice with and without cachexia and littermates were assessed by qRT-PCR. Error bars represent SEM. *, $P < 0.05$; **, $P < 0.01$; ***, $P < 0.001$. Combined data are from three independent analyses ($n = 1-5$).

loss-of-function approach to the analysis of the roles of FAP⁺ stromal cells in normal tissues. Their wide distribution could have rendered this approach relatively uninformative if severe,

generalized stress resulted from their depletion. However, DTX-treated BAC transgenic mice initially appeared free from signs of severe distress such as piloerection, hunching, and altered

patterns of movement despite the conspicuous changes affecting food intake, body weight, skeletal muscle mass, and hematopoiesis (Figs. 3 and 4). It has been shown previously that muscle atrophy caused by a range of metabolic challenges is mediated by the actions of atrogin-1 and MuRF1 (Sandri et al., 2004). One pathway leading to the expression of these E3 ligases is AcvRIIB signaling in response to certain TGF- β family members (Zhou et al., 2010). Accordingly, either increased levels of Mstn or activin A or reduced levels of Fst, an inhibitor of these molecules, may lead to muscle wasting (Zimmers et al., 2002; Costelli et al., 2008). With respect to the latter, the Fst288 isoform, which binds to the extracellular matrix and thus acts locally, is both necessary and sufficient for maintenance of normal muscle mass. This is demonstrated by the comparison between the wasted *Fst*^{+/-} mouse and the normal muscle mass of mice expressing only the Fst288 isoform (Lee et al., 2010; Brown et al., 2011). Therefore, finding that FAP⁺ cells of skeletal muscle not only produced this isoform but also were the only source of Fst biosynthesis in this tissue (Fig. 3, H and I) could explain how the loss of this cell led to a reduction in muscle mass. The stabilization of muscle mass and cessation of AcvRIIB signaling despite the continued decrease of FAP⁺ stromal cells and Fst is consistent with the compensatory lowering of Mstn expression seen by day 22 (Fig. 3 E). The decrease in Lama2 expression in the mice depleted of FAP⁺ stromal cells also could have contributed to muscle atrophy, as the *dy*^{3K}/*dy*^{3K} mouse model of congenital muscular dystrophy with Lama2 deficiency exhibits skeletal muscle wasting secondary to elevated atrogin-1 and MuRF1 and proteasome-mediated protein degradation (Carmignac et al., 2011).

A second acute abnormality in mice depleted of FAP⁺ stromal cells was a hypocellular bone marrow, which represented decreased frequencies of pro-Es, MEPs, pro-Bs, and CLPs (Fig. 4, A and B). The explanation for these changes became apparent when FAP⁺ stromal cells from bone marrow were found to express Cxcl12 and KitL (Fig. 4, E, F, and H), characteristics of the previously described CAR cell, conditional depletion of which resulted in a similar hematopoietic phenotype (Omatsu et al., 2010). Although the observed phenotypes are similar, there are subtle differences, such as the increase in multipotent progenitors seen with the depletion of FAP⁺ cells but not with the loss of Cxcl12-expressing cells. This finding may reflect the existence of FAP⁻ and Cxcl12-single expressing cells, as indicated by the occurrence of acute liver necrosis with the ablation of Cxcl12⁺ cells (Omatsu et al., 2010) but normal liver function tests in mice depleted of FAP⁺ cells (Table 1). FAP⁺ cells from the bone marrow also expressed *Lepr*, a marker of perivascular cells that produce KitL (Ding et al., 2012). The absence of an effect on HSCs in the DTX-treated mice, however, may be accounted for by the incomplete ablation of FAP⁺ cells and the absence of FAP expression by endothelial cells, which are the second major source of KitL in the bone marrow (Ding et al., 2012). Furthermore, although FAP⁺ cells express *Lepr*, this does not exclude the presence of *Lepr*-expressing cells that are FAP⁻, which would

also not be affected in this system, thus explaining the lack of an HSC phenotype. These other sources may comprise rare populations in the CD45⁻FAP⁻ sorted population and so expression of *Lepr*, *KitL*, and *Cxcl12* would not appear. However, as the whole bone marrow level of Cxcl12 and KitL was reduced upon FAP⁺ cell ablation (Fig. 4, E and F), it can be concluded that the FAP⁺ cells do constitute a major source of these factors.

The finding that depletion of FAP⁺ stromal cells led to loss of muscle mass and anemia predicted that disease-associated alterations in FAP⁺ cells could lead to similar phenotypes. Because both cachexia and anemia are common syndromes associated with cancer, there was the intriguing possibility that the cachexia and anemia caused by cancer may have a common etiological basis involving this cell. This possibility was supported by the finding of reduced FAP-dependent tissue bioluminescence of the cachectic mice bearing the C26 colon carcinoma (Fig. 5) and the fact that the C26-induced abnormality of FAP⁺ cells in skeletal muscle and bone marrow was accompanied by a diminution of their tissue-specific functions of producing Fst, Lama2, Cxcl12, and KitL, which could account for the occurrence of cachexia and anemia (Fig. 6). That these changes in the FAP⁺ cells were not an artifact of a transplantable tumor model was shown by finding a comparable abnormality of FAP⁺ stromal cells from the skeletal muscle and bone marrow of cachectic and anemic mice bearing spontaneous PDA (Fig. 7). The DTX-mediated ablation of FAP⁺ cells demonstrates that these changes may be causative rather than correlative (Figs. 3 and 4) and indicates that these two experimental systems may share a common etiology. The presence of anemia in noncachectic KPC animals and the loss of FAP⁺ cells in the bone marrow of these animals indicate that in this slower developing tumor model, there is a loss of FAP⁺ cells from the bone marrow before the skeletal muscle. Further work will be needed to elucidate the factors from the tumor which bring about these changes and how they may differentially affect bone marrow and skeletal muscle FAP⁺ cells.

Many studies have focused on the cytokines TNF and IL-6 as mediating wasting syndromes associated with cancer (Tisdale, 2009). There is, however, an imperfect correlation between elevated cytokines and the occurrence of these pathologies (Mantovani et al., 2000), and neutralizing these cytokines has not suppressed their occurrence (Wiedenmann et al., 2008). Recent preclinical and clinical studies of cancer cachexia have shown alterations of the muscular dystrophy-associated dystrophin glycoprotein complex (Acharyya et al., 2005) and excessive signaling by the AcvRIIB of skeletal muscle myocytes (Benny Klimek et al., 2010; Zhou et al., 2010). Moreover, Fst was found to be reduced in the muscle of cachectic rats with a transplanted model of cancer cachexia (Costelli et al., 2008), further implicating the AcvRIIB pathway. This study extends these studies by finding a cellular basis of reduced Fst in skeletal muscle of tumor-bearing cachectic mice. Furthermore, as the FAP⁺ cell also is the source of Lama2 in skeletal muscle, its alteration offers an explanation for the abnormality

of the dystroglycan complex in cancer cachexia (Acharyya et al., 2005). Similarly, the hypoproliferative bone marrow of cancer patients with normocytic, normochromic anemia (Spivak, 2005) is compatible with the hematopoietic phenotype of cancer-bearing mice in which FAP⁺ cells are depleted from the bone marrow (Fig. 7 C). Collectively, these observations add to the increasing awareness of the capacity of tumors to affect distal sites, as has been reported for the development of the metastatic niche (Peinado et al., 2011), and emphasize that these alterations of the FAP⁺ stromal cell in normal tissues are as important to consider as are the functions of the FAP⁺ cell in the tumor stroma.

However, the present study does not determine whether the cancer-induced loss of FAP-expressing stromal cells in normal tissues reflects cell death, as occurs in the DTX-treated BAC transgenic mice, migration to another site, perhaps contributing to the accumulation of FAP⁺ stromal cells in the tumors, or development into a FAP-negative stromal cell that has lost a capacity for the production of tissue-specific proteins, such as those required for the maintenance of skeletal muscle and bone marrow. Our study also has not identified what is produced by tumors to alter the tissue FAP⁺ stromal cell or whether the alteration is reversible after elimination of a cancer. Based on the finding of a persistent decrease of FAP⁺ stromal cells in skeletal muscle after DTX-mediated depletion, the restoration of FAP⁺ stromal cells may be predicted to occur only if the tumor-induced loss reflects a reversible developmental process.

From the perspective of whether the killing of FAP⁺ cells might be a viable therapeutic approach for overcoming tumoral immune suppression, this study indicates that a more nuanced strategy will be required. FAP⁺ stromal cells reside in many normal tissues, and in at least two of these they have essential functions, findings which preclude adopting this simplistic clinical strategy. The revelation of the complexity of the FAP⁺ stromal cell, however, is offset not only by the uncovering of a potentially new stromal cell lineage with roles in tissue homeostasis, but also by the unexpected discovery that two paraneoplastic syndromes, cachexia and anemia, may be caused by the idiopathic alteration of these stromal cells from skeletal muscle and bone marrow.

MATERIALS AND METHODS

BAC clone modification and purification. A 206-kb BAC clone (RP23-16A15) containing the *fap* gene was purchased from BACPAC resources. The BAC was modified by introducing the reporter construct at the start ATG of the *fap* gene by homologous recombination. Undamaged BAC was purified using a CsCl gradient purification.

Mice. All experiments were performed under guidelines of and were approved by the UK Home Office and the animal ethics committee of the University of Cambridge. Transgenic mice were generated via pronuclear injection of BAC DNA into 0.5-d fertilized ova of F1(C57BL/6 × CBA) donors. Mice positive for the transgene were identified by PCR and backcrossed at least 10 times to the C57BL/6 Tyr^{-/-} background. DTX was administered in all experiments at a dose of 25 ng/g, and the C26 cells were subcutaneously inoculated into the flank of appropriate animals (2×10^6 cells per mouse).

RNA-Seq. Total RNA from the sorted cells was prepared using the PureLink RNA Mini kit from Invitrogen. The MessageAmp II aRNA kit (Ambion) was used for amplification of 100–500 ng total RNA according to the manufacturer's instructions. The double-strand cDNA was subjected to library preparation using the Illumina mRNA sample preparation kit (Illumina) directly to the 3' adenylation step and according to manufacturer's protocol. Sequence-by-synthesis single-end reads of 72-bp length using the SBS Sequencing kit (Illumina) were generated on the Genome Analyzer Iix (Illumina).

In vivo imaging. Mice were intraperitoneally injected with 150 µg/g body weight D-luciferin (PerkinElmer) and imaged using IVIS (Xenogen). Whole body images were acquired for 20 s at 1.5-cm stage height, and organs were imaged for 20 s at 0.5-cm stage height. Data were analyzed using Living Image (PerkinElmer).

Flow cytometry. Single cell suspensions were made and stained as previously described (Kraman et al., 2010). Cell sorts were performed using the MoFlo system (Dako). Antibodies were obtained from eBioscience except CD4 H29.19 (BD), α-hFAP AF3715 (R&D Systems), and the biotinylated mouse α-sheep IgG GT-34 (Sigma-Aldrich).

Computational methods. RNA-Seq data were mapped to the iGenomes UCSC mm9 reference using the bowtie2 short read mapper (Langmead and Salzberg, 2012), and tophat2 was used to map junction reads. Cufflinks2 (Trapnell et al., 2010) was used to calculate gene FPKM expression values with bias adjustment. RPKM values were calculated using count data from htseq-count version 0.5.3p4 in Python version 2.7. CD4⁺ T cell subset RNA-Seq data were obtained from the study by Wei et al. (2011; GEO series no. GSE20898). Expression levels for RPKM were then discretized into lowly expressed (LE) and highly expressed categories, as previously described (Hebenstreit et al., 2011). Genes with RPKM values that were LE were then filtered out of clustering and correlation calculations (which were calculated using Pearson's r^2 and Spearman's ρ), whereas genes with no expression were filtered from FPKM correlations.

qRT-PCR analysis. mRNA was extracted using TRIzol (Invitrogen) and analyzed by quantitative real-time PCR using the SuperScript III Platinum One-Step qRT-PCR system (Invitrogen). Values for each gene were normalized to the relative quantity of *Tbp* mRNA in each sample. Primers probes were obtained from Applied Biosystems.

ELISA. Protein was extracted as previously described (Omatsu et al., 2010). Concentrations of KitL and Cxcl12 were measured using Quantikine kits (R&D Systems) according to the manufacturer's instructions.

Microscopy. Femurs were fixed overnight in 10% NBF and then decalcified in 10% EDTA for 21 d, changing the solution daily. The femurs were then cut in half and dehydrated in sucrose solution for 48 h before being moved through increasing concentrations of OCT before freezing in OCT. Slides were prepared and stained as previously described (Kraman et al., 2010). Antibodies used were Osteocalcin mOC(1–20) (Takara Bio Inc.), Osteopontin P-18 (Santa Cruz Biotechnology, Inc.), Lama2 4H8-2 (Enzo Life Sciences), and FAP AF3715 (R&D Systems).

Western blot. Protein was extracted as previously described (Costelli et al., 2008). Protein was separated by NuPAGE (Invitrogen) transferred to nitrocellulose using the iBlot system (Invitrogen) and probed with antibodies against 1 µg/ml Fst (Santa Cruz Biotechnology, Inc.) and 1 µg/ml β-actin (Abcam) before probing with IRDye secondary antibodies (LI-COR Biosciences). Membranes were scanned and fluorescence was quantified using the Odyssey fluorescence imaging system (LI-COR Biosciences) according to the manufacturer's instructions.

Blood biochemistry. Blood was collected under terminal anesthesia by cardiac puncture into heparinized tubes. Plasma was collected and analyzed using the Analyst III (Woodley Equipment) according to the manufacturer's instructions.

Statistics. Where two groups were compared, this was performed using Student's *t* test, and where three groups were compared, an ANOVA test was used with the Tukey post test to determine significant differences between individual groups. *P*-values < 0.05 were considered significant.

Online supplemental material. Table S1 shows the alignment statistics and replicate correlations for RNA-Seq data. Online supplemental material is available at <http://www.jem.org/cgi/content/full/jem.20122344/DC1>.

This work was supported by the Wellcome Trust, the Ludwig Institute for Cancer Research, Cancer Research UK, the Anthony Cerami and Anne Dunne Foundation for World Health, the Lustgarten Foundation, the J.B. and Millicent Kaye Fellowship, and the Clinician Investigator Program at the University of British Columbia, Canada.

The authors declare no competing financial interests.

Submitted: 19 October 2012

Accepted: 29 April 2013

REFERENCES

- Acharyya, S., M.E. Butchbach, Z. Sahenk, H. Wang, M. Saji, M. Carathers, M.D. Ringel, R.J. Skipworth, K.C. Fearon, M.A. Hollingsworth, et al. 2005. Dystrophin glycoprotein complex dysfunction: a regulatory link between muscular dystrophy and cancer cachexia. *Cancer Cell*. 8:421–432. <http://dx.doi.org/10.1016/j.ccr.2005.10.004>
- Aertgeerts, K., I. Levin, L. Shi, G.P. Snell, A. Jennings, G.S. Prasad, Y. Zhang, M.L. Kraus, S. Salakian, V. Sridhar, et al. 2005. Structural and kinetic analysis of the substrate specificity of human fibroblast activation protein alpha. *J. Biol. Chem.* 280:19441–19444. <http://dx.doi.org/10.1074/jbc.C500092200>
- Bauer, S., M.C. Jendro, A. Wadle, S. Kleber, F. Stenner, R. Dinser, A. Reich, E. Faccin, S. Gödde, H. Dinges, et al. 2006. Fibroblast activation protein is expressed by rheumatoid myofibroblast-like synoviocytes. *Arthritis Res. Ther.* 8:R171. <http://dx.doi.org/10.1186/ar2080>
- Benny Klimek, M.E., T. Aydogdu, M.J. Link, M. Pons, L.G. Koniaris, and T.A. Zimmers. 2010. Acute inhibition of myostatin-family proteins preserves skeletal muscle in mouse models of cancer cachexia. *Biochem. Biophys. Res. Commun.* 391:1548–1554. <http://dx.doi.org/10.1016/j.bbrc.2009.12.123>
- Bodine, S.C., E. Latres, S. Baumhueter, V.K. Lai, L. Nunez, B.A. Clarke, W.T. Poueymirou, F.J. Panaro, E. Na, K. Dharmarajan, et al. 2001. Identification of ubiquitin ligases required for skeletal muscle atrophy. *Science*. 294:1704–1708. <http://dx.doi.org/10.1126/science.1065874>
- Brokopp, C.E., R. Schoenauer, P. Richards, S. Bauer, C. Lohmann, M.Y. Emmert, B. Weber, S. Winnik, E. Aikawa, K. Graves, et al. 2011. Fibroblast activation protein is induced by inflammation and degrades type I collagen in thin-cap fibroatheromata. *Eur. Heart J.* 32:2713–2722. <http://dx.doi.org/10.1093/eurheartj/ehq519>
- Brown, M.L., L. Bonomi, N. Ungerleider, J. Zina, F. Kimura, A. Mukherjee, Y. Sidis, and A. Schneyer. 2011. Follistatin and follistatin like-3 differentially regulate adiposity and glucose homeostasis. *Obesity (Silver Spring)*. 19:1940–1949. <http://dx.doi.org/10.1038/oby.2011.97>
- Carmignac, V., R. Quéré, and M. Durbej. 2011. Proteasome inhibition improves the muscle of laminin α 2 chain-deficient mice. *Hum. Mol. Genet.* 20:541–552. <http://dx.doi.org/10.1093/hmg/ddq499>
- Chang, H.Y., J.T. Chi, S. Dudoit, C. Bondre, M. van de Rijn, D. Botstein, and P.O. Brown. 2002. Diversity, topographic differentiation, and positional memory in human fibroblasts. *Proc. Natl. Acad. Sci. USA*. 99:12877–12882. <http://dx.doi.org/10.1073/pnas.162488599>
- Coll, A.P., I.S. Farooqi, and S. O'Rahilly. 2007. The hormonal control of food intake. *Cell*. 129:251–262. <http://dx.doi.org/10.1016/j.cell.2007.04.001>
- Costelli, P., M. Muscaritoli, A. Bonetto, F. Penna, P. Reffo, M. Bossola, G. Bonelli, G.B. Doglietto, F.M. Baccino, and F. Rossi Fanelli. 2008. Muscle myostatin signalling is enhanced in experimental cancer cachexia. *Eur. J. Clin. Invest.* 38:531–538. <http://dx.doi.org/10.1111/j.1365-2362.2008.01970.x>
- Ding, L., T.L. Saunders, G. Enikolopov, and S.J. Morrison. 2012. Endothelial and perivascular cells maintain haematopoietic stem cells. *Nature*. 481:457–462. <http://dx.doi.org/10.1038/nature10783>
- Dolznic, H., N. Schweifer, C. Puri, N. Kraut, W.J. Rettig, D. Kerjaschki, and P. Garin-Chesa. 2005. Characterization of cancer stroma markers: in silico analysis of an mRNA expression database for fibroblast activation protein and endosialin. *Cancer Immun.* 5:10.
- Dvorak, H.F. 1986. Tumors: wounds that do not heal. Similarities between tumor stroma generation and wound healing. *N. Engl. J. Med.* 315:1650–1659. <http://dx.doi.org/10.1056/NEJM198612253152606>
- Eager, R.M., C.C. Cunningham, N. Senzer, D.A. Richards, R.N. Raju, B. Jones, M. Uprichard, and J. Nemunaitis. 2009a. Phase II trial of talabostat and docetaxel in advanced non-small cell lung cancer. *Clin. Oncol. (R. Coll. Radiol.)* 21:464–472. <http://dx.doi.org/10.1016/j.clon.2009.04.007>
- Eager, R.M., C.C. Cunningham, N.N. Senzer, J. Stephenson Jr., S.P. Anthony, S.J. O'Day, G. Frenette, A.C. Pavlick, B. Jones, M. Uprichard, and J. Nemunaitis. 2009b. Phase II assessment of talabostat and cisplatin in second-line stage IV melanoma. *BMC Cancer*. 9:263. <http://dx.doi.org/10.1186/1471-2407-9-263>
- Evans, W.J., J.E. Morley, J. Argilés, C. Bales, V. Baracos, D. Guttridge, A. Jatoi, K. Kalantar-Zadeh, H. Lochs, G. Mantovani, et al. 2008. Cachexia: a new definition. *Clin. Nutr.* 27:793–799. <http://dx.doi.org/10.1016/j.clnu.2008.06.013>
- Garin-Chesa, P., L.J. Old, and W.J. Rettig. 1990. Cell surface glycoprotein of reactive stromal fibroblasts as a potential antibody target in human epithelial cancers. *Proc. Natl. Acad. Sci. USA*. 87:7235–7239. <http://dx.doi.org/10.1073/pnas.87.18.7235>
- Glass, D.J. 2010. Signaling pathways perturbing muscle mass. *Curr. Opin. Clin. Nutr. Metab. Care*. 13:225–229. <http://dx.doi.org/10.1097/MCO.0b013e32833862df>
- Gomes, M.D., S.H. Lecker, R.T. Jagoe, A. Navon, and A.L. Goldberg. 2001. Atrogin-1, a muscle-specific F-box protein highly expressed during muscle atrophy. *Proc. Natl. Acad. Sci. USA*. 98:14440–14445. <http://dx.doi.org/10.1073/pnas.251541198>
- Hebenstreit, D., M. Fang, M. Gu, V. Charoensawan, A. van Oudenaarden, and S.A. Teichmann. 2011. RNA sequencing reveals two major classes of gene expression levels in metazoan cells. *Mol. Syst. Biol.* 7:497. <http://dx.doi.org/10.1038/msb.2011.28>
- Hebenstreit, D., A. Deonaraine, M.M. Babu, and S.A. Teichmann. 2012. Duel of the fates: the role of transcriptional circuits and noise in CD4+ cells. *Curr. Opin. Cell Biol.* 24:350–358. <http://dx.doi.org/10.1016/j.cob.2012.03.007>
- Hingorani, S.R., L. Wang, A.S. Multani, C. Combs, T.B. Deramandt, R.H. Hruban, A.K. Rustgi, S. Chang, and D.A. Tuveson. 2005. Trp53R172H and KrasG12D cooperate to promote chromosomal instability and widely metastatic pancreatic ductal adenocarcinoma in mice. *Cancer Cell*. 7:469–483. <http://dx.doi.org/10.1016/j.ccr.2005.04.023>
- Hofheinz, R.D., S.E. al-Batran, F. Hartmann, G. Hartung, D. Jäger, C. Renner, P. Tanswell, U. Kunz, A. Amelsberg, H. Kuthan, and G. Stelhe. 2003. Stromal antigen targeting by a humanised monoclonal antibody: an early phase II trial of sibtrotuzumab in patients with metastatic colorectal cancer. *Onkologie*. 26:44–48. <http://dx.doi.org/10.1159/000069863>
- Huang, S., R. Fang, J. Xu, S. Qiu, H. Zhang, J. Du, and S. Cai. 2011. Evaluation of the tumor targeting of a FAP α -based doxorubicin prodrug. *J. Drug Target.* 19:487–496. <http://dx.doi.org/10.3109/1061186X.2010.511225>
- Kennedy, G.C. 1950. The hypothalamic control of food intake in rats. *Proc. R. Soc. Lond. B Biol. Sci.* 137:535–549. <http://dx.doi.org/10.1098/rspb.1950.0065>
- Kraman, M., P.J. Bambrough, J.N. Arnold, E.W. Roberts, L. Magiera, J.O. Jones, A. Gopinathan, D.A. Tuveson, and D.T. Fearon. 2010. Suppression of antitumor immunity by stromal cells expressing fibroblast activation protein-alpha. *Science*. 330:827–830. <http://dx.doi.org/10.1126/science.1195300>
- Langmead, B., and S.L. Salzberg. 2012. Fast gapped-read alignment with Bowtie2. *Nat. Methods*. 9:357–359. <http://dx.doi.org/10.1038/nmeth.1923>

- LeBeau, A.M., W.N. Brennen, S. Aggarwal, and S.R. Denmeade. 2009. Targeting the cancer stroma with a fibroblast activation protein-activated promelittin protoxin. *Mol. Cancer Ther.* 8:1378–1386. <http://dx.doi.org/10.1158/1535-7163.MCT-08-1170>
- Lee, S.J., and A.C. McPherron. 2001. Regulation of myostatin activity and muscle growth. *Proc. Natl. Acad. Sci. USA.* 98:9306–9311. <http://dx.doi.org/10.1073/pnas.151270098>
- Lee, S.J., L.A. Reed, M.V. Davies, S. Girgenrath, M.E. Goad, K.N. Tomkinson, J.F. Wright, C. Barker, G. Ehrmantraut, J. Holmstrom, et al. 2005. Regulation of muscle growth by multiple ligands signaling through activin type II receptors. *Proc. Natl. Acad. Sci. USA.* 102:18117–18122. <http://dx.doi.org/10.1073/pnas.0505996102>
- Lee, S.J., Y.S. Lee, T.A. Zimmers, A. Soleimani, M.M. Matzuk, K. Tsuchida, R.D. Cohn, and E.R. Barton. 2010. Regulation of muscle mass by follistatin and activins. *Mol. Endocrinol.* 24:1998–2008. <http://dx.doi.org/10.1210/me.2010-0127>
- Levy, M.T., G.W. McCaughan, C.A. Abbott, J.E. Park, A.M. Cunningham, E. Müller, W.J. Rettig, and M.D. Gorrell. 1999. Fibroblast activation protein: a cell surface dipeptidyl peptidase and gelatinase expressed by stellate cells at the tissue remodelling interface in human cirrhosis. *Hepatology.* 29:1768–1778. <http://dx.doi.org/10.1002/hep.510290631>
- Mantovani, G., A. Macciò, L. Mura, E. Massa, M.C. Mudu, C. Mulas, M.R. Lusso, C. Madeddu, and A. Dessì. 2000. Serum levels of leptin and pro-inflammatory cytokines in patients with advanced-stage cancer at different sites. *J. Mol. Med.* 78:554–561. <http://dx.doi.org/10.1007/s001090000137>
- Mauro, A. 1961. Satellite cell of skeletal muscle fibers. *J. Biophys. Biochem. Cytol.* 9:493–495. <http://dx.doi.org/10.1083/jcb.9.2.493>
- McFarlane, C., E. Plummer, M. Thomas, A. Hennebray, M. Ashby, N. Ling, H. Smith, M. Sharma, and R. Kambadur. 2006. Myostatin induces cachexia by activating the ubiquitin proteolytic system through an NF-kappaB-independent, FoxO1-dependent mechanism. *J. Cell. Physiol.* 209:501–514. <http://dx.doi.org/10.1002/jcp.20757>
- McPherron, A.C., and S.J. Lee. 1997. Double muscling in cattle due to mutations in the myostatin gene. *Proc. Natl. Acad. Sci. USA.* 94:12457–12461. <http://dx.doi.org/10.1073/pnas.94.23.12457>
- Niedermeyer, J., M. Kriz, F. Hilberg, P. Garin-Chesa, U. Bamberger, M.C. Lenter, J. Park, B. Viertel, H. Püschner, M. Mauz, et al. 2000. Targeted disruption of mouse fibroblast activation protein. *Mol. Cell. Biol.* 20:1089–1094. <http://dx.doi.org/10.1128/MCB.20.3.1089-1094.2000>
- Niedermeyer, J., P. Garin-Chesa, M. Kriz, F. Hilberg, E. Mueller, U. Bamberger, W.J. Rettig, and A. Schnapp. 2001. Expression of the fibroblast activation protein during mouse embryo development. *Int. J. Dev. Biol.* 45:445–447.
- Omatsu, Y., T. Sugiyama, H. Kohara, G. Kondoh, N. Fujii, K. Kohno, and T. Nagasawa. 2010. The essential functions of adipo-osteogenic progenitors as the hematopoietic stem and progenitor cell niche. *Immunity.* 33:387–399. <http://dx.doi.org/10.1016/j.immuni.2010.08.017>
- Park, J.E., M.C. Lenter, R.N. Zimmermann, P. Garin-Chesa, L.J. Old, and W.J. Rettig. 1999. Fibroblast activation protein, a dual specificity serine protease expressed in reactive human tumor stromal fibroblasts. *J. Biol. Chem.* 274:36505–36512. <http://dx.doi.org/10.1074/jbc.274.51.36505>
- Peinado, H., S. Lavotshkin, and D. Lyden. 2011. The secreted factors responsible for pre-metastatic niche formation: old sayings and new thoughts. *Semin. Cancer Biol.* 21:139–146. <http://dx.doi.org/10.1016/j.semcancer.2011.01.002>
- Rettig, W.J., P.G. Chesa, H.R. Beresford, H.J. Feickert, M.T. Jennings, J. Cohen, H.F. Oettgen, and L.J. Old. 1986. Differential expression of cell surface antigens and glial fibrillary acidic protein in human astrocytoma subsets. *Cancer Res.* 46:6406–6412.
- Sandri, M., C. Sandri, A. Gilbert, C. Skurk, E. Calabria, A. Picard, K. Walsh, S. Schiaffino, S.H. Lecker, and A.L. Goldberg. 2004. Foxo transcription factors induce the atrophy-related ubiquitin ligase atrogin-1 and cause skeletal muscle atrophy. *Cell.* 117:399–412. [http://dx.doi.org/10.1016/S0092-8674\(04\)00400-3](http://dx.doi.org/10.1016/S0092-8674(04)00400-3)
- Santos, A.M., J. Jung, N. Aziz, J.L. Kissil, and E. Puré. 2009. Targeting fibroblast activation protein inhibits tumor stromagenesis and growth in mice. *J. Clin. Invest.* 119:3613–3625. <http://dx.doi.org/10.1172/JCI38988>
- Scott, A.M., G. Wiseman, S. Welt, A. Adjei, F.T. Lee, W. Hopkins, C.R. Divgi, L.H. Hanson, P. Mitchell, D.N. Gansen, et al. 2003. A Phase I dose-escalation study of sibroutzumab in patients with advanced or metastatic fibroblast activation protein-positive cancer. *Clin. Cancer Res.* 9:1639–1647.
- Spivak, J.L. 2005. The anaemia of cancer: death by a thousand cuts. *Nat. Rev. Cancer.* 5:543–555. <http://dx.doi.org/10.1038/nrc1648>
- Szymczak, A.L., C.J. Workman, Y. Wang, K.M. Vignali, S. Dilioglou, E.F. Vanin, and D.A. Vignali. 2004. Correction of multi-gene deficiency in vivo using a single 'self-cleaving' 2A peptide-based retroviral vector. *Nat. Biotechnol.* 22:589–594. <http://dx.doi.org/10.1038/nbt957>
- Tanaka, Y., H. Eda, T. Tanaka, T. Udagawa, T. Ishikawa, I. Horii, H. Ishitsuka, T. Kataoka, and T. Taguchi. 1990. Experimental cancer cachexia induced by transplantable colon 26 adenocarcinoma in mice. *Cancer Res.* 50:2290–2295.
- Tisdale, M.J. 2009. Mechanisms of cancer cachexia. *Physiol. Rev.* 89:381–410. <http://dx.doi.org/10.1152/physrev.00016.2008>
- Trapnell, C., B.A. Williams, G. Pertea, A. Mortazavi, G. Kwan, M.J. van Baren, S.L. Salzberg, B.J. Wold, and L. Pachter. 2010. Transcript assembly and quantification by RNA-Seq reveals unannotated transcripts and isoform switching during cell differentiation. *Nat. Biotechnol.* 28:511–515. <http://dx.doi.org/10.1038/nbt.1621>
- Wei, G., B.J. Abraham, R. Yagi, R. Jothi, K. Cui, S. Sharma, L. Narlikar, D.L. Northrup, Q. Tang, W.E. Paul, et al. 2011. Genome-wide analyses of transcription factor GATA3-mediated gene regulation in distinct T cell types. *Immunity.* 35:299–311. <http://dx.doi.org/10.1016/j.immuni.2011.08.007>
- Wiedenmann, B., P. Malfertheiner, H. Friess, P. Ritch, J. Arseneau, G. Mantovani, F. Caproni, E. Van Cutsem, D. Richel, M. DeWitte, et al. 2008. A multicenter, phase II study of infliximab plus gemcitabine in pancreatic cancer cachexia. *J. Support. Oncol.* 6:18–25.
- Zhou, X., J.L. Wang, J. Lu, Y. Song, K.S. Kwak, Q. Jiao, R. Rosenfeld, Q. Chen, T. Boone, W.S. Simonet, et al. 2010. Reversal of cancer cachexia and muscle wasting by ActRIIB antagonism leads to prolonged survival. *Cell.* 142:531–543. <http://dx.doi.org/10.1016/j.cell.2010.07.011>
- Zimmers, T.A., M.V. Davies, L.G. Koniaris, P. Haynes, A.F. Esquela, K.N. Tomkinson, A.C. McPherron, N.M. Wolfman, and S.J. Lee. 2002. Induction of cachexia in mice by systemically administered myostatin. *Science.* 296:1486–1488. <http://dx.doi.org/10.1126/science.1069525>